Task 3.1

Title

Innovative technologies

Projects (presented on the following pages)

Two-phase flow phenomena in turbines and pump-turbines operating in synchronous condenser mode
Elena Vagnoni, Loïc Andolfatto, Renaud Guillaume, Pierre Leroy, François Avellan

DuoTurbo: First Product and Pilote Test Sites
Daniel Biner, Laurent Rapillard, Loïc Andolfatto, Vlad Hasmatuchi, Shadya Martignoni, François Avellan, Cécile Münch-Alligné

GPU-SPHEROS: A GPU-Accelerated 3-D Finite Volume Particle Method solver
Siamak Alimirzazadeh, Ebrahim Jahanbakhsh, Audrey Maertens, Sebastian Leguizamón, François Avellan

RENOVHydro: Development of a Decision Making Assistant for Hydropower Project Potential Evaluation and Optimization
Christian Landry, Christophe Nicolet, João Gomes Pereira Junior, Loic Andolfatto, Carlo Todde, Julien Derivaz, François Avellan

Pressure oscillation test rig
Anthony Gaspoz, Manuel Almeida, Christophe Nicolet, Samuel Rey-Mermet

Direct-marketing remuneration and flexibility of small hydro
Jérémy Schmid ,Shadya Martignoni, Cécile Münch-Alligné

Recent Advances in Numerical Predictions for Off-Design Conditions in Hydraulic Turbomachines
Ernesto Casartelli, Luca Mangani, David Roos Launchbury, Armando Del Rio

Hydrokinetic turbine farm: challenges & expectations
Olivier Pacot, Jérémy Schmid, Shadya Martignoni, Jean Decaix, Nino Brunner, Cécile Münch-Alligné

Configuring a hydrokinetic turbine farm by CFD
Olivier Pacot, Jérémy Schmid, Shadya Martignoni, Jean Decaix, Nino Brunner, Cécile Münch-Alligné

Calibration of borehole failure models using inverse problem methods
Asmae dahrabou, Benoit Valley, Andres Alcolea, Peter Meier, Florentin Ladner, Frederic Guinot

Boreholes stability issues in ultra-deep geothermal production
Antonio Salazar, Leonid Germanovic, Carlo Rabaiotti & Paul Hardegger

Empirical model for the estimation of a Francis turbine complete characteristics curve
Joao Gomes, Loic Andolfatto, François Avellan

Cavitation modelling in GPU-Spheros
Audrey Maertens, Ebrahim Jahanbakhsh, François Avellan

SCCER SoE
SWISS COMPETENCE CENTER for ENERGY RESEARCH
SUPPLY of ELECTRICITY

SCCER-SoE Annual Conference 2018

LMH Laboratory for Hydraulic Machines

EPFL ÉCOLE POLYTECHNIQUE FÉDÉRALE DE LAUSANNE

Supported by:
Schweizerische Eidgenossenschaft
Confédération suisse
Confederazione Svizzera
Confederaziun svizra

Swiss Confederation

Innosuisse – Swiss Innovation Agency

Two-phase flow phenomena in turbines and pump-turbines operating in synchronous condenser mode

E. Vagnoni, L. Andolfatto, R. Guillaume, P. Leroy, F. Avellan

Energy context

Importance of the reactive power in the grid:

US northeast and Canada blackout, August 2003

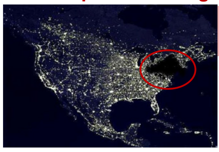

Reactive power shortage

⬇

Lack in balancing the voltage instability in the grid

Increasing demand of reactive power supply/absorption:

- Environmental and policy changes
- Changes in the generation mix
- International transit trade of electricity

Synchronous condenser mode operation:

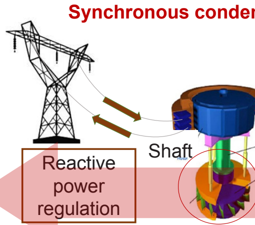

Francis turbine or pump-turbine operating in synchronous condenser mode

Objective

Prediction of the **mechanical power consumption** of a pump-turbine during the operation in **synchronous condenser mode**.

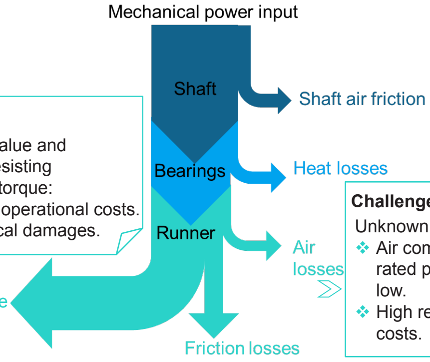

Challenge:
Significant value and oscillating resisting mechanical torque:
- Increase operational costs.
- Mechanical damages.

Challenge:
Unknown losses:
- Air compressor rated power too low.
- High replacement costs.

Experimental tests

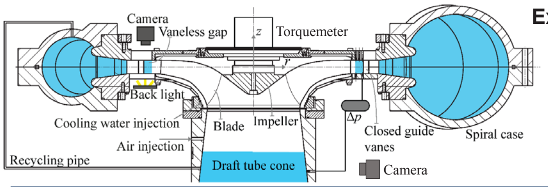

Configuration of a pump-turbine in synchronous condenser mode:
- Guide vanes are closed.
- Compressed air injected in the draft tube to keep the water level below the runner.
- Cooling water discharge.
- Recycling pipe to reduce the pressure in the spiral case.

Results

- Study of torque stability correlated to the air-water ring dynamics.
- Flow phenomenology and torque can be classified in 4 regimes depending on the densimetric Froude number.
- Regime 1 is stable and influenced by the pressure.
- Regime 2 is strongly unstable: operation in this regime should be avoided.
- Regime 3 and 4 are stable. The torque can be predicted as a function of the densimetric Froude number.

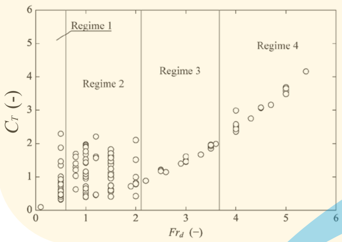

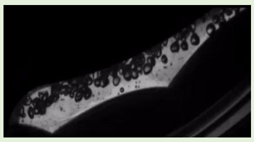

- Study of the two-phase flow phenomenology.
- Flow dynamics as a function of the densimetric Froude number.
- Strong influence on the pressure and torque fluctuations.

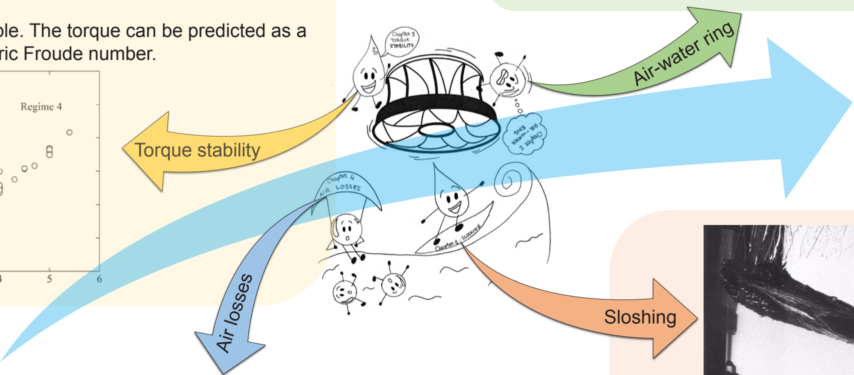

- Study of the air diffusion into the water volume.
- Theoretical model validated on oxygen concentration measurements.
- The mass flow rate of lost air can be predicted as a function of the pressure, the cooling discharge and the densimetric Froude number.

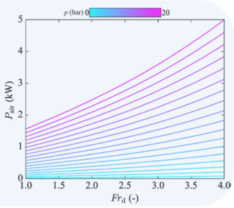

- Study of the free surface dynamics.
- Rotating gravity wave at the first azimuthal wave number m = 1.
- Wave breaking is observed by increasing the densimetric Froude number.
- Torque fluctuation are not correlated with this flow oscillation.

References

1. E. Vagnoni et al., (2018), "Rotating air-water ring in the vaneless gap of a pump-turbine operating in condenser mode," Int. Journal of Multiphase Flow 105, 112-121. doi: 10.1016/j.ijmultiphaseflow.2018.03.022.
2. E. Vagnoni et al., (2018), "Experimental investigation of the sloshing motion of the water free-surface in the draft tube of a Francis turbine operating in synchronous condenser mode," Experiments in Fluids, 59(6):95. doi: 10.1007/s00348-018-2552-x.
3. E. Vagnoni et al., (2018), "Interaction of a rotating two-phase flows with the torque stability of a reversible pump-turbine operating in condenser mode," Int. Journal of Multiphase Flow.

SCCER SoE
SWISS COMPETENCE CENTER for ENERGY RESEARCH
SUPPLY of ELECTRICITY

SCCER-SoE Annual Conference 2018

Hes·so// VALAIS WALLIS School of Engineering

Supported by:
Schweizerische Eidgenossenschaft
Confédération suisse
Confederazione Svizzera
Confederaziun svizra

Swiss Confederation

Innosuisse – Swiss Innovation Agency

DuoTurbo : First Product and Pilot Test Sites

D. Biner [1], L. Rapillard [1], L. Andolfatto [2], V. Hasmatuchi [1], S. Martignoni, F. Avellan [2], C. Münch-Alligné [1]

[1]*HES-SO Valais//Wallis, School of Engineering, Hydroelectricity Group, Sion, daniel.biner@hevs.ch*
[2]*EPFL, Laboratory for Hydraulic Machines, Lausanne*

Context

- Recovering hydraulic energy lost in **drinking water networks**
- Modular in-line "plug and play" turbine from **5 to 25 kW**
- No environmental impact
- Low investment costs

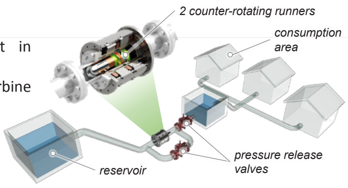

Mechanical concept

Based on the experience gathered during the prototype phase, a new mechanical concept was established. The achieved mechanical robustness enables the possibility of long term operation at the pilot sites. The mechanical complexity was significantly reduced and a modularity to target a wide discharge range is provided.

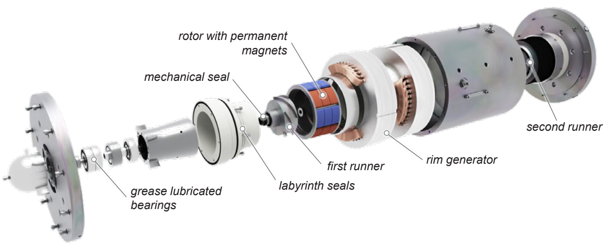

Hydraulic design

Hydraulic characteristics

The runners of the first product were designed for the pilot site of Savièse. According to different design limitations, a reasonable design point was chosen.

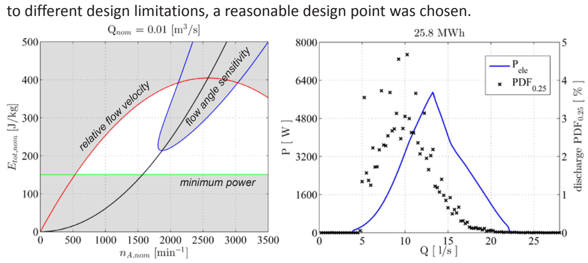

Numerical simulations

The runner design was iteratively established by means of CFD simulations in order to maximize the turbine's performance. A hydraulic efficiency of more than 85 % is achieved.

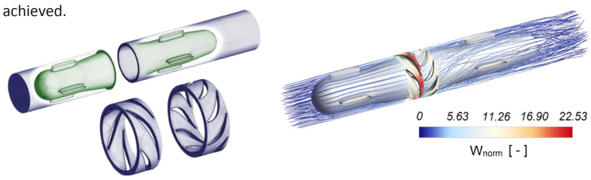

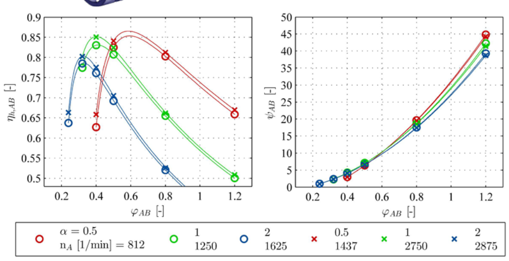

Project

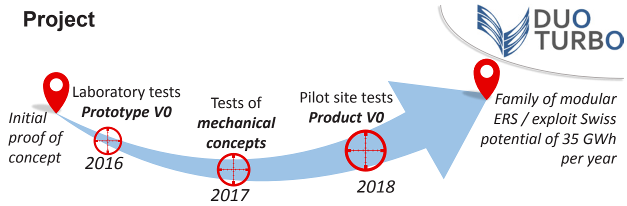

Laboratory tests

Detailed experimental investigations have been carried out on the hydraulic test rig of the HES-SO Valais//Wallis. A maximum regenerated electrical power of 6.5 kW was measured, reaching a global efficiency of nearly 60 % that corresponds to an enhancement of 14 % compared to the prototype V0. Additionally, the automation of the entire system, including the maximum power point tracking algorithm (MPPT), was successfully tested.

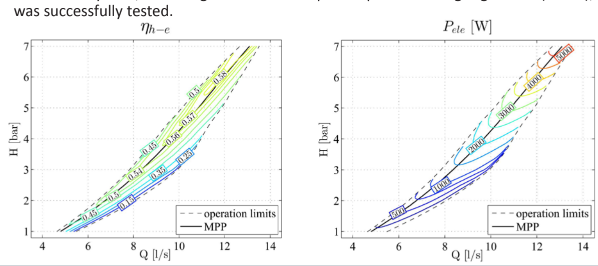

Pilot test sites

In 2018 two pilot sites are targeted for long term tests of the first DuoTurbo products. On both sites, detailed data of hydraulic, electrical and mechanical measurands will be collected.

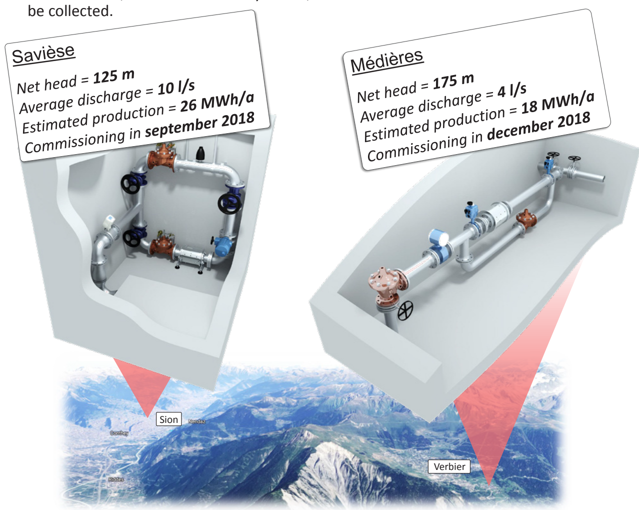

Conclusion

To sum up the main achievements of the DuoTurbo project, ending in June 2018, a successful development of a new energy recovery system for future installations on many potential drinking water facilities can be mentioned. Passing from the prototype phase to the first operational product, significant enhancements concerning the turbine's lifecycle and performance were achieved. At the two pilot sites equipped this year, the robustness, expected efficiency and system stability under long-term operating conditions will be assessed.

References

- D. Biner, V. Hasmatuchi, D. Violante, S. Richard, S. Chevailler, L. Andolfatto, F. Avellan, C. Münch, **"Engineering and Performance of DuoTurbo: Microturbine with Counter-Rotating Runners"**, *28nd IAHR Symposium - Grenoble*, July 2016.

Development team of Duo Turbo (CTI Nr. 17197.1 PFEN-IW)

HES-SO Valais//Wallis:
D. Biner, S. Luisier, S. Martignoni, D. Violante , V. Hasmatuchi, S. Richard, C. Cachelin, L. Rapillard, S. Chevailler, C. Münch-Alligné

EPFL LMH:
L. Andolfatto, V. Berruex, F. Avellan

Industrial partners:
Telsa SA, Jacquier-Luisier SA, Valelectric Farner SA

Hes·so// VALAIS WALLIS Haute Ecole d'Ingénierie Hochschule für Ingenieurwissenschaften
LMH Laboratory for Hydraulic Machines EPFL
VALELECTRIC FARNER SA
TELSA ELECTROTECHNIQUE
Jacquier & Luisier SA Atelier mecanique

SCCER-SoE Annual Conference 2016

In cooperation with the CTI

GPU-SPHEROS: A GPU-Accelerated 3-D Finite Volume Particle Method solver

S Alimirzazadeh, E Jahanbakhsh, A Maertens, S Leguizamón, F Avellan

Introduction

GPU-SPHEROS is a GPU-accelerated particle-based solver based on Finite Volume Particle Method (**FVPM**) which inherits desirable features of both Smoothed Particle Hydrodynamics (SPH) and mesh-based Finite Volume Method (FVM) and is able to simulate the interaction between fluid, solid and silt [1]. With GPU-SPHEROS, the goal is to perform a industrial size setup simulations of hydraulic machines.

Software flowchart

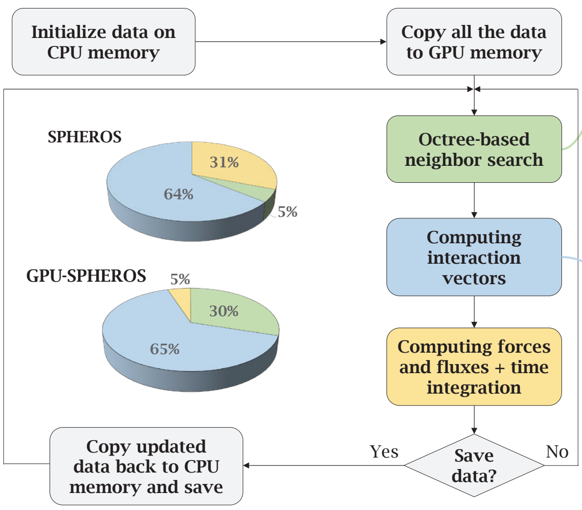

Speedup

- On NVIDIA Tesla P100, GPU-SPHEROS is almost **5.5x faster** than the CPU version running on a dual CPU node with two Intel® Xeon® E5-2690 v4 Broadwell CPUs and also more than 6x faster compared to a machine with two Intel® Xeon® E5-2660 v2 Ivy-Bridge CPUs.
- Overall throughput reaches higher than **3x10^5** particles per second on **NVLink-based Tesla P100 SXM-2 16 GB**.

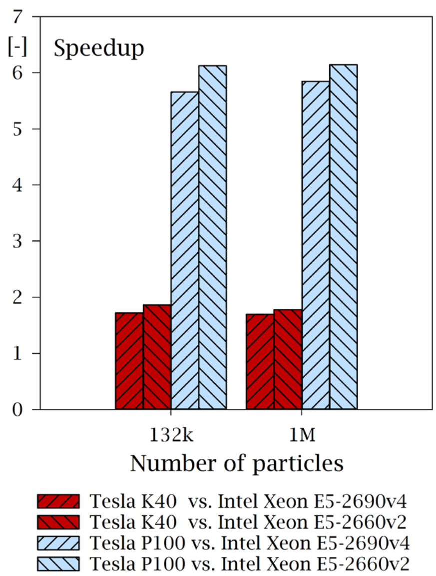

Octree-based neighbor search

- **Memory access efficiency** is a key point for GPU applications to be able to get a good performance.
- The data has been reordered using **space filling curves** (SFCs) to improve memory access.
- An octree-based neighbor search algorithm has been implemented to find the neighbor particles.
- A highly optimized kernel has been implemented for parallel distance check between the particles.

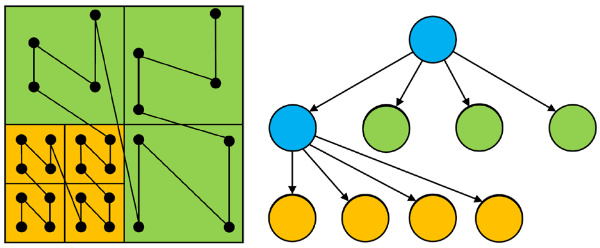

Computing interaction vectors

- GPU-SPHEROS has been developed based on spherical-supported kernels.
- A fixed-size pre-allocated memory is used for computing interaction vectors procedure and the access order considered to have a coalesced memory access to minimize memory transactions.
- The particles are grouped into smaller batches and the computations are divided into different batches in which they are performed in parallel for each batch and the batches themselves are released sequentially.

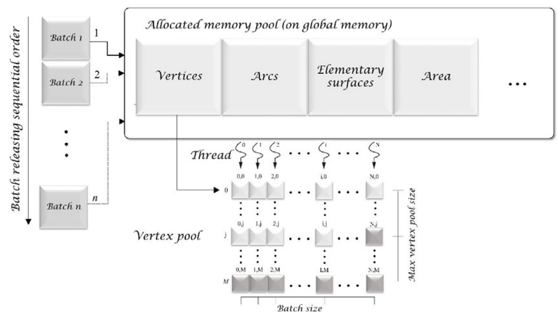

Case study

- **Turbulent** free jet deviated by rotating Pelton buckets has been simulated by GPU-SPHEROS to verify the solver validity. There is a good agreement between the predicted and measured torque.

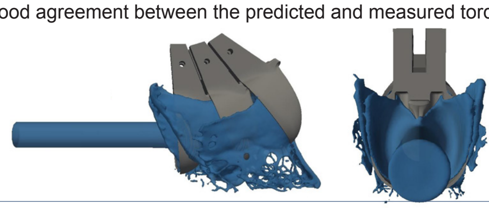

References

[1] E. Jahanbakhsh, A. Maertens, N. J. Quinlan, C. Vessaz, F. Avellan, Exact finite volume particle method with spherical-support kernels, *Comput. Methods Appl. Mech. Engrg.* 317 (2017) 102–127

[2] S. Alimirzazadeh, E. Jahanbakhsh, A. Maertens, S. Leguizamon, F. Avellan, GPU-Accelerated 3-D finite volume particle method, *Computers & Fluids*. 171 (2018) 79–93

SCCER SoE
SWISS COMPETENCE CENTER for ENERGY RESEARCH
SUPPLY of ELECTRICITY

SCCER-SoE Annual Conference 2018

RENOV Hydro

Supported by:
Schweizerische Eidgenossenschaft
Confédération suisse
Confederazione Svizzera
Confederaziun svizra
Swiss Confederation
Innosuisse – Swiss Innovation Agency

RENOVHydro: Development of a Decision Making Assistant for Hydropower Project Potential Evaluation and Optimization

Christian Landry, Christophe Nicolet, João Gomes Pereira Junior, Loïc Andolfatto, Carlo Todde, Julien Derivaz, François Avellan

Motivation

The RENOVHydro project is dedicated to the **renovation** of an existing hydroelectric power plant with a systematic assessment of a **high number of civil and electromechanical potential modifications**. **Energy and economic indicators** such as annual energy generation, annual amount of turbined/pumped water, investment cost, profitability and ancillary services for each renovation option can be analyzed to identify technical trends according to **political, economic and environmental contexts.**

1. SIMSEN model import

The SIMSEN simulation software enables to model an entire power plant including **hydraulic, mechanical and electrical system** and their related control systems. **Realistic performance hill charts** of the turbine were generated with a polynomial bi-variate functions base on Hermite polynomials and can be selected in a database for **Francis, Pelton, Kaplan turbines and pump-turbines**.

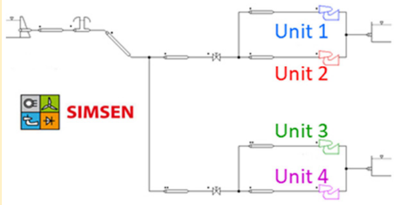

Example of hydraulic power plant with 4 Francis turbines

2. Selection of renovation options

Many civil engineering and hydroelectric options are available (add new penstock, increase reservoir storage, upgrade the turbine, add variable speed, …). For each renovation option, **a pre-dimensioning** and a **cost estimation** are computed.

Methodology

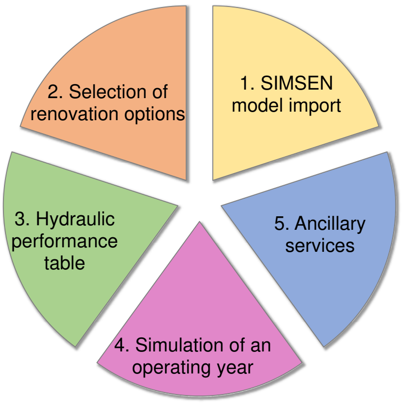

3. Hydraulic performance table

A hydraulic performance table defines the **most efficient distribution of units for all power set points** and all upstream water levels. To evaluate the hydraulic power plant performances over the entire operating range, each unit combination and each guide vane opening combination are evaluated for a given upstream water level.

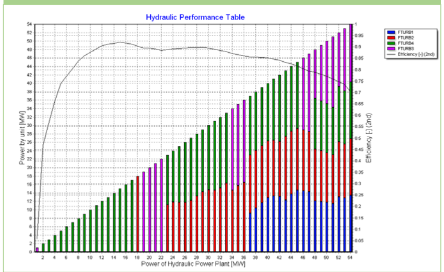

5. Ancillary services

The performance offered by the renovation options regarding **interaction with the electrical power networks**, such as primary and secondary control capabilities, is evaluated to determine the **maximum load step response compatible** with Transmission System Operator requirements.

4. Simulation of an operating year

The best performance of each renovation option is computed with a mathematical optimization approach (**Mixed-Integer Linear Programming algorithm**). **Energy and economic indicators** for each renovation option are quantified to identify technical trends according to political, economic and environmental contexts.

Input data for simulation of an operating year

- **The electricity market price and hydrology time history** for a reference year.
- **Power and level limitations** during a year.
- **Maintenance periods** and possible **outage** over the whole **concession duration**.

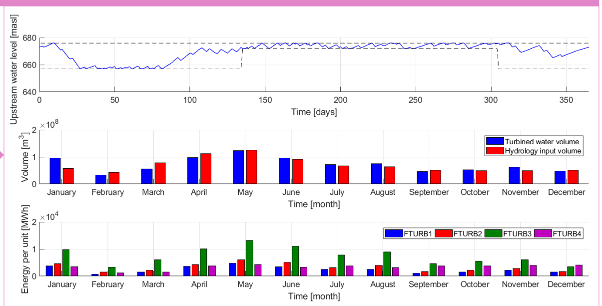

Energy indicators: Annual energy: 195.9 [GWh], Turbined flow: 836.5 [Mm³]
Economic indicators: Annual profit: 7.19 [MCHF], Profitability: 36.67 [CHF/MWh]

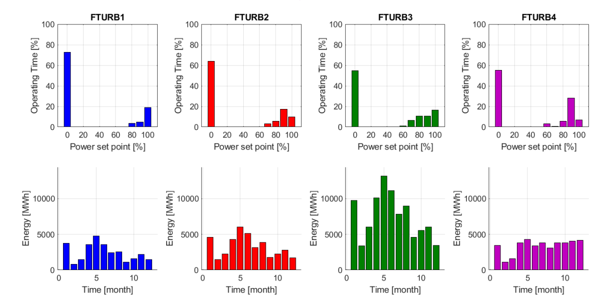

Acknowledgments

The RENOVHydro project is granted by CTI, Commission for Technology and Innovation (Grant funding 19343.1 PFEN-IW) and by SFOE, Swiss Federal Office of Energy (Grant funding SI/501436-01).

ÉCOLE POLYTECHNIQUE FÉDÉRALE DE LAUSANNE
Power Vision Engineering
groupe e
LABORATOIRE DE CONSTRUCTIONS HYDRAULIQUES
FMV

SCCER SoE
SWISS COMPETENCE CENTER for ENERGY RESEARCH
SUPPLY of ELECTRICITY

SCCER-SoE Annual Conference 2018

Hes·so VALAIS WALLIS
Haute Ecole d'Ingénierie
Hochschule für Ingenieurwissenschaften

Supported by:
Schweizerische Eidgenossenschaft
Confédération suisse
Confederazione Svizzera
Confederaziun svizra

Swiss Confederation

Innosuisse – Swiss Innovation Agency

Pressure oscillation test rig

Anthony Gaspoz, Samuel Rey-Mermet HESSO Valais-Wallis

Motivation

As the the prices on the electrical market are still low, the hydropower asset managers want to reduce their maintenance costs. With the help of risk management and materials ageing laws, they can make better decision to lower their global costs in the long term.
The Swiss Federal Council has evaluated that the investment necessary to maintain the hydropower capacity of Switzerland till 2050 amounts to 30 billions of CHF.

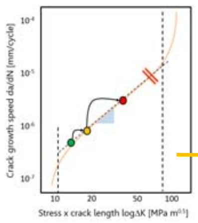

Paris ageing law

Risk based mangement

30 billions of CHF 2010-2050*

*Swiss Federal Council estimation
https://www.parlament.ch/fr/ratsbetrieb/suche-curia-vista/geschaeft?AffairId=20143501

Pipeline

The pipeline length is calculated to obtain the mechanical resonance in the middle of it according to the speed of the valve.

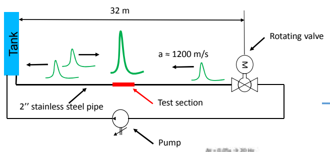

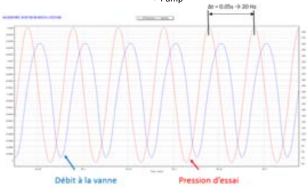

Simulation of the pressure and valve position with time

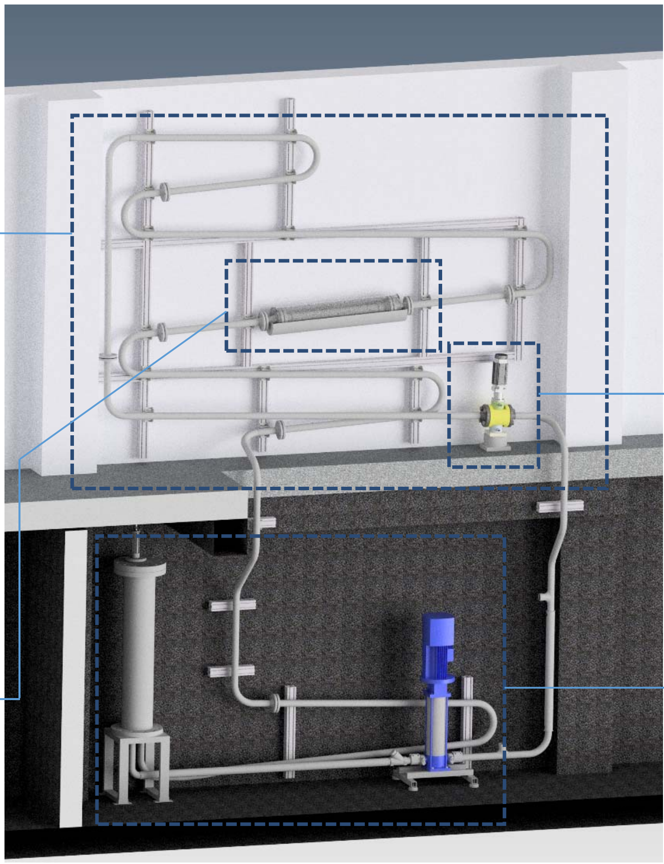

Rotating valve

The rotating valve has a diameter of 2", a nominal pressure of 100 bars and a rotating speed of 1500 rpm. It will create pressure oscillations in the specimen pipe.
With its speed it will be possible to simulate 50 years of operations pressure fluctuations in less than 2 days.

Crack growth in specimen pipe

The specimen pipe is located in the middle of the pipeline where the mechanical resonance occurs.

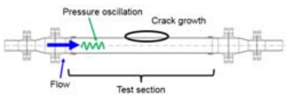

The pipe contains machined cracks that will grow under the pressure oscillations according to the Paris law or a a thin section where the fatigue will occur.

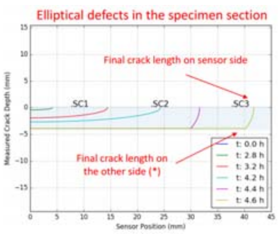

Profile of a crack growing in a test bar and monitored by an Eddy current sensor

A specific Eddy current sensor (Sensima) will monitor the the crack growing speed. In the thin section, the stress variations will be measured by a dedicated gauge and the fatigue will be calculated based on the Wöhler law.

Water recirculating system

As the test rig is a close loop system, it is necessary to recirculate water into it. Thus the test rig comprises a variable speed pump (up to 15m³/s, PN12) and a tank (70 l, PN40) in the basement of the building.

Results and benefits

The test rig will be operating in December.

Benefits of the in lab test rig
Proof of concept of the fatigue monitoring (accumulation of damage due to pressure oscillations)
Proof of concept of the crack growth monitoring (in water, in real time, with real cracks)
Study of the ageing laws

Benefits for assets management
Better ageing law → better risk prediction

Partners

Power Vision Engineering   SENSIMA inspection

SCCER SoE
SWISS COMPETENCE CENTER for ENERGY RESEARCH
SUPPLY of ELECTRICITY

SCCER-SoE Annual Conference 2018

Hes·so VALAIS WALLIS
School of Engineering

Supported by:
Schweizerische Eidgenossenschaft
Confédération suisse
Confederazione Svizzera
Confederaziun svizra
Swiss Confederation
Innosuisse – Swiss Innovation Agency

Direct-marketing remuneration and flexibility of small hydro

Jérémy Schmid ,Shadya Martignoni, Cécile Münch-Alligné
HES-SO Valais, School of Engineering, Hydroelectricity Group, CH-1950 Sion, Switzerland, jeremy.schmid@hevs.ch

Context

Following the acceptance of the energy strategy 2050, the energy law changes came into force on 1 January 2018, such as the Ordinance on the encouragement of renewable electricity generation (OEneR).

As part of this revision, the system of compensation at cost price of the injected current (RPC) is adapted into a system of compensation of injection (SRI1) based on two models of remuneration including direct marketing. This incentive model implies that the operators of installations must henceforth sell their electricity on the energy market.

This revision will therefore push some distributors with small hydropower plants to better predict their production and to stall at the best market price. The case study is carried out of a 2MW hydropower plant located in Icogne (VS).

Direct-marketing remuneration

- Have to sell the electricity themselves on the market.
- The quantity of energy produced is traded on the market by the operator itself or through a direct distributor.
- The goal is to encourage to produce and operate renewable installations according to the market.

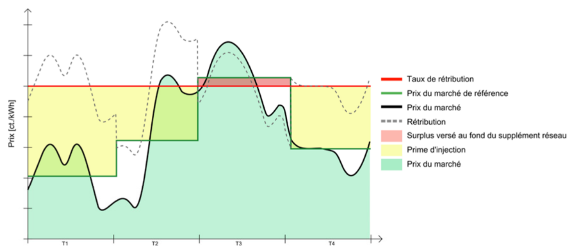

Representation of direct-marketing price

Impacts of the direct-marketing

1) If the market price < the reference price => the distributor lose

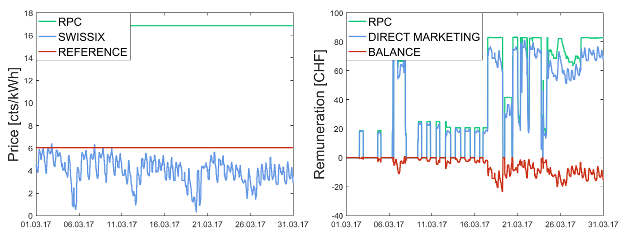

2) If the market price > the reference price => the distributor can win

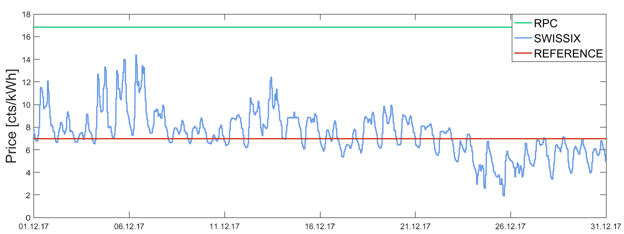

Flexibility of the hydropower plant management

Low peak water flow period

- Simple optimisation with ON/OFF programme
- Low cost management with daily schedule
- Based on historical market price analysis
- Flexibility with turbine flow and reservoir variation level

=> Increase average cost-price by 10-15%

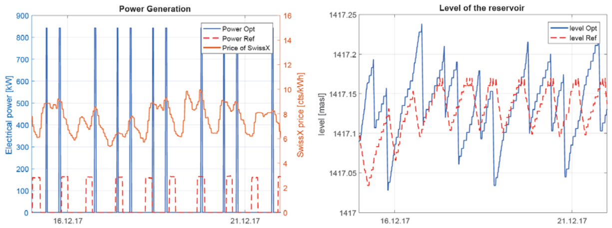

High peak water flow period

- Flexible production when the constraints are not reached
- Forced to produce continuously when input flow is high
- Based on historical market price analysis
- Flexibility with turbine flow and reservoir variation level

- => Increase average cost-price by 1%

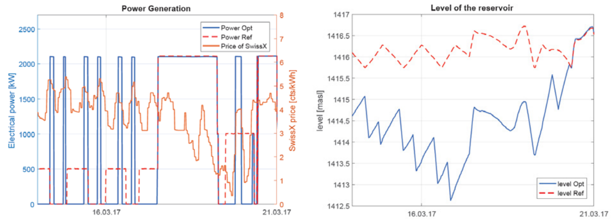

Conclusion

- Goal of direct-marketing is to encourage small hydropower plants to comply with the electricity market and to provide their injection.
- The flexibility can reduce the impact of the direct-marketing on the hydropower plant remuneration with an increase of the remuneration price by 10-15 % in winter and can absorb all the losses of all year.
- The winter period is more predictable and flexible. It's also easier to make some gains although the production represent a small part of the whole year production.

Acknowledgements

esr énergies sion région FMV energy center

References

[1] Office Fédéral de l'énergie OEFN : Loi du 30 septembre 2016 sur l'énergie (LEne) (Etat le 1er janvier 2018). RO 2017 6839. 2017. Bern. **[2]** Office Fédéral de l'énergie OFEN : Ordonnance du 1er novembre 2017 sur l'encouragement de la production d'électricité issue d'énergies renouvelables (OEneR) (Etat le 1er janvier 2018). RO 2017 7783. 2017. Bern. **[3]** Office fédéral de l'énergie OFEN : Commercialisation directe – Fiche technique. 22 novembre 2017. Bern.

SCCER SoE
SWISS COMPETENCE CENTER for ENERGY RESEARCH
SUPPLY of ELECTRICITY

SCCER-SoE Annual Conference 2018

Supported by:
Schweizerische Eidgenossenschaft
Confédération suisse
Confederazione Svizzera
Confederaziun svizra

Swiss Confederation

Innosuisse – Swiss Innovation Agency

Recent Advances in Numerical Predictions for Off-Design Conditions in Hydraulic Turbomachines

E. Casartelli, L. Mangani, D. Roos Launchbury, A. Del Rio

Introduction

Simulations of off-design conditions in hydraulic machines, especially in unstable operating points, are difficult to perform because the conditions are dominated by unguided, highly turbulent flow in the vaneless spaces which often cannot be accurately predicted using conventional turbulence models. This is due to the fact that the most commonly used models, such as k-Epsilon and the Shear Stress Transport (SST) model assume isotropic turbulence. This assumption is not valid for many flow problems but seems to have an especially large influence in pump turbine instability simulations. Figure 1 shows a close-up of such a typical S-shaped operating curve. The quantity k_{cm1} is a normalised flow rate and k_{u1} is a normalised machine speed.

The goal of the current efforts is to implement advanced turbulence models in a coupled solver and improve their efficiency and robustness for pump turbine instability simulations.
This work will be of direct importance in upcoming large-scale simulations as part of the SCCER-FURIES project.

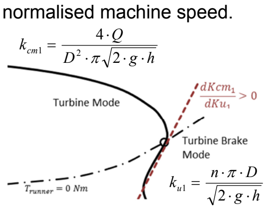

Figure 1: Unstable Operating Range

Second-Moment Closure Turbulence Models

Explicit Algebraic Reynolds Stress Models (EARSM)
EARSMs do not solve additional transport equations but try to reconstruct the unknown stress tensor through an algebraic equation based on the velocity gradients. Two different formulations were implemented, one by Menter [4] and one by Hellsten [2].

Full Reynolds Stress Models
The full Reynolds stress model solves an equation for each component of the Reynolds stress tensor along with an equation for the turbulence length scale, leading to a total of 7 equation in addition to the momentum and pressure equations. Wilcox' Stress Omega model [5] was implemented using the Baseline modifications by Menter [3].

Convergence Improvements for Reynolds Stress Models

The Reynolds stress transport equations are usually solved sequentially. In order to improve convergence and stability, in this work the Reynolds stress equations are solved in a coupled fashion, leading to a 6x6 block matrix structure. This procedure was applied to a simple backward facing step test case and it could be shown that convergence of all solution variables is reached using fewer iterations compared to the segregated version. The segregated version also suffered from oscillations at the reattachment point of the flow that inhibited convergence. Figures 2a and 2b show the improved convergence of the momentum, pressure and Reynolds stress variables respectively.

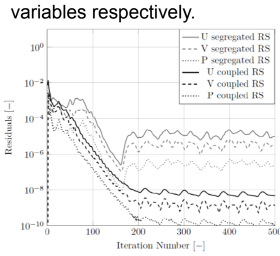

Figure 2a: Pressure/Momentum Convergence

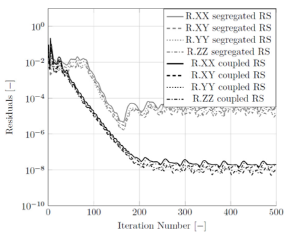

Figure 2b: Reynolds Stress Convergence

Simulation Results

NACA0012 with Full Reynolds Stress Model
To validate the implementation of the full Reynolds stress model the solution of the wing tip vortex around a NACA0012 profile was compared to measurements by Chow et al. [1]. The crossflow velocity $\sqrt{v^2 + w^2}/U_\infty$ along a span-wise line through the vortex core is evaluated at different positions downstream of the wing. Figure 4a shows the comparison between SST, RSM and measurements. The agreement between simulation and measurement is very good and a large improvement over the SST model can be observed. Figure 4b shows a position very far downstream (582%). The vortex has essentially disappeared for the SST model, while RSM is able to sustain the vortex strength. This model will be applied to a full pump turbine simulation in the near future.

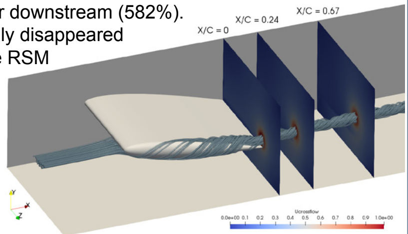

Figure 3: NACA0012 Tip Vortex

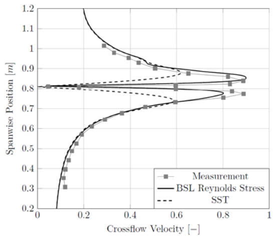

Figure 4a: Crossflow Velocity at X/C = 0.67

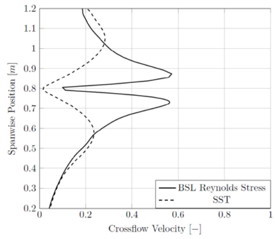

Figure 4b: Crossflow Velocity at X/C = 5.82

Unstable Pump Turbine with EARSM
A validated EARSM model was applied to a 360° unsteady pump turbine simulation in an unstable operating range and compared to our own measurements. It can clearly be seen that while the SST model misses the instability entirely, the more advanced EARSM model is able to accurately reproduce the entire S-shaped instability region. This finding underlines the importance of turbulence modelling for the simulation of off-design and unstable operating points and shows the validity of the implemented model.

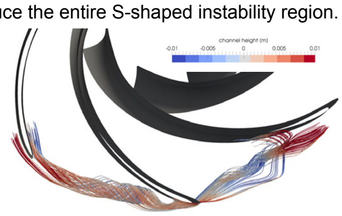

Figure 5: Vortex Formation in Vaneless Space of Pump Turbine

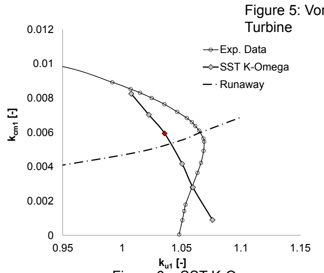

Figure 6a: SST K-Omega

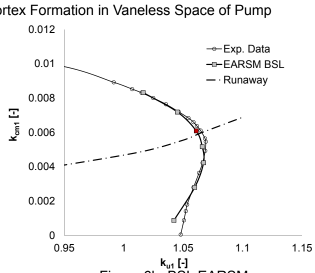

Figure 6b: BSL EARSM

References

[1] Chow, J. S., Zilliac, G. G., and Bradshaw, P., "Mean and Turbulence Measurements in the Near Field of a Wingtip Vortex," AIAA Journal, Vol. 35, No. 10, pp. 1561–1567.
[2] Hellsten, A., "New Advanced k-omega Turbulence Model for High-Lift Aerodynamics", AIAA Journal, Vol. 43, No. 9, 2005, pp. 1857-1869.
[3] Menter, F. R., "Two-Equation Eddy-Viscosity Turbulence Models for Engineering Applications," AIAA Journal, Vol. 32, No. 8, 1994, pp. 1598-1605.
[4] Menter, F. R., Garbaruk, A.V, and Egorov, Y., "Explicit Algebraic Reynolds Stress Models for Anisotropic Wall-Bounded Flows", Progress in Flight Physics, Vol. 3, 2012, pp. 89-104
[5] Wilcox, D. C., "Turbulence Modeling for CFD", 3rd edition, DCW Industries, Inc., La Canada CA, 2006.

SWISS COMPETENCE CENTER for ENERGY RESEARCH
SUPPLY of ELECTRICITY

SCCER-SoE Annual Conference 2018

Supported by:
Schweizerische Eidgenossenschaft
Confédération suisse
Confederazione Svizzera
Confederaziun svizra

Swiss Confederation

Innosuisse – Swiss Innovation Agency

Hydrokinetic turbine farm: challenges & expectations

O. Pacot[1], J. Schmid[1], S. Martignoni[1], J. Decaix[1], N. Brunner[2], C. Münch-Alligné[1]
[1]HES-SO Valais, School of Engineering, Hydroelectricity Group, CH-1950 Sion, Switzerland, olivier.pacot@hevs.ch
[2]Stahleinbau Gmbh, Talstrasse 30, CH-3922 Stalden, Switzerland

Context

- The performance of the first hydrokinetic (Hkt) turbine prototype [1] with a power of 1 kW has been tested and validated for real conditions in Lavey [2].
- To increase the power output, several hydrokinetic turbines will be assembled.
- The small size of the hydrokinetic turbine make it possible to implant it in shallow river: 4-5 meters water height.

Objective:

- Develop and install a cost-effective hydrokinetic farm with a power output of 10 kW in the tailrace channel in Lavey.

Lavey Pilot Site & Potential

This pilot site of Lavey was selected because of the following characteristics [2-3]:

- Artificial channel with a filtered water thanks to the upstream hydropower plant
- Available flow speed between 0.5 and 1.7 m/s
- Averaged flow speed of 1.4 m/s

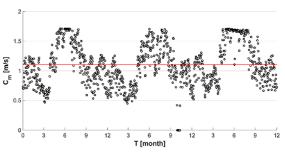

Site Potential [MWh]		
Hkt Power	Rotor Steady Speed	Rotor Variable Speed
1.4 kW	18.59	19.91
2.0 kW	26.00	27.88
3.3 kW	20.40	21.85

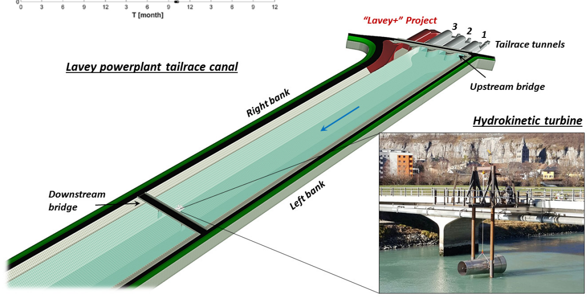

Farm Configuration Options

Config. 7 machines (1.4 kW): 2-3-2

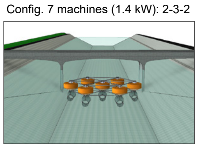

Config. 5 machines (2.0 kW): 2-3

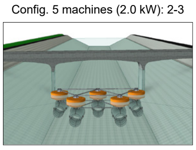

Config. 3 machines (3.3 kW): 1-2

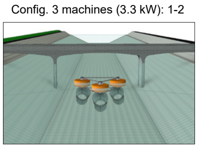

Zoom on the modular structure

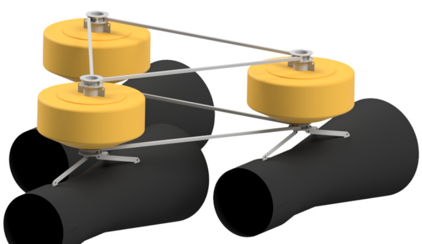

Single Hkt Performance & Long Operation Challenge

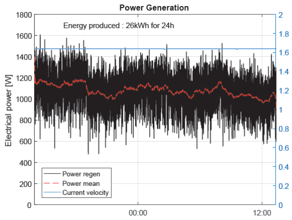

- Good overall performance of the Hkt in real conditions.
- The power generated during one full day test reached 26 kWh.
- Presently, the rotation frequency is maintained constant. However, variable rotation speed will be implemented.

- Future challenge: how the natural algae, grass and leaves will alter the global performance of the Hkt?
- And how can we design the machine to minimize this sticking problem?

Cost Estimation

- To estimate the cost of the farm, the latter is decomposed in 3 parts: the cost to build the machine, the structure cost and the cost of all electronic and electric equipment.
- The table below shows the estimated prices of a single Hkt and the farm. The prices are normalized by the price of a single 1.4 kW Hkt.

Hkt Max Power	7 x 1.4 kW	5 x 2.0 kW	3 x 3.3 kW
Machine	0.73	0.89	1.00
Farm Structure	0.16	0.18	0.23
Electric & Electronics	0.11	0.11	0.14
Cost of a single Hkt	**1.00**	**1.18**	**1.36**
Cost of a farm	**7.00**	**5.91**	**4.09**

- The increase of the Hkt power increases the price of the machine. However, it is shown that with the reduced number of Hkt required, the configuration using 3 Hkt is the most financially advantageous.

Conclusions

- The performance of a single hydrokinetic turbine in real conditions during several days showed that the expected power output is reached.
- The modular and stable structure allow to implant and adapt the farm configuration to any kind of environment.
- With this assembly of turbines, it is expected to reach a power output of 10 kW and produce 25 MWh.
- The cost estimation showed that a single 3.3 kW Hkt is 36% more expensive then a 1.4 kW Hkt. However, the farm using only three 3.3 kW Hkt is the most advantageous.

References

[1] C. Münch, S. Richard, A. Gaspoz, V. Hasmatuchi, N. Brunner, "New Prototype of a Kinetic Turbine of Artificial Channels" Advances in Hydroinformatics, Springer, Singapore, 2018, pp. 981-996.

[2] C. Münch, J. Schmid, S. Richard, A. Gaspoz, N. Brunner, V. Hasmatuchi, "Experimental Assessment of a New Kinetic Turbine Performance for Artificial Channels" Water 2018, Volume 10, Issue 3, 311.

[3] V. Hasmatuchi, A. Gaspoz, L. Rapillard, N. Brunner, S. Richard, S. Chevailler, C. Münch-Alligné, 2016, "Open-air laboratory for a new isokinetic turbine prototype", Annual conference, SCCER SoE, Sion.

Office fédéral de l'énergie OFEN

SCCER SoE
SWISS COMPETENCE CENTER for ENERGY RESEARCH
SUPPLY of ELECTRICITY

SCCER-SoE Annual Conference 2018

Hes·so Valais Wallis
School of Engineering

Supported by:
Schweizerische Eidgenossenschaft
Confédération suisse
Confederazione Svizzera
Confederaziun svizra

Swiss Confederation

Innosuisse – Swiss Innovation Agency

Configuring a hydrokinetic turbine farm by CFD

O. Pacot[1], J. Schmid[1], S. Martignoni[1], J. Decaix[1], N. Brunner[2], C. Münch-Alligné[1]

[1]*HES-SO Valais, School of Engineering, Hydroelectricity Group, CH-1950 Sion, Switzerland, olivier.pacot@hevs.ch*
[2]*Stahleinbau Gmbh, Talstrasse 30, CH-3922 Stalden, Switzerland*

Context

- The performance of the first hydrokinetic (Hkt) turbine prototype [1] with a power of 1 kW has been tested and validated for real conditions in Lavey [2].
- To increase the power output, the idea is to assemble several hydrokinetic turbines as a farm, which requires to investigate the influence of the machines between each other.

Objective:

- Configure a hydrokinetic farm to reach an output power of 10 kW by a cost-effective CFD approach.

Hydrokinetic Turbine Model

To minimise the amount of computational resources and to speed up the computations, a model of the Hkt is used [3]. This model mimics the pressure drops experienced by the fluid from the runner. This approach has the advantage to avoid to compute the unsteady flow between the stationary and rotating domains.

Unsteady CFD

- Entire geometry of one Hkt
- Non-viscous fluid
- RS interface: «Frozen»
- Computations done for several λ.
- ~5 million elements (1 Hkt)

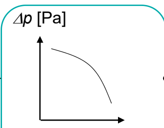

Turbine Model Loss Coefficient

$$K_{\mathrm{loss}} = \frac{A_{\mathrm{r}}^2 \Delta p}{\frac{1}{2}\rho Q_{\mathrm{r}}^2}$$

Turbine Model Source Term

$$\begin{cases} \boldsymbol{S}_{\mathrm{M,x}} = -\frac{\mu}{K_{\mathrm{perm}}^{\mathrm{S}}} U_{\mathrm{x}} - K_{\mathrm{loss}}^{\mathrm{S}} \frac{\rho}{2} |\boldsymbol{U}| U_{\mathrm{x}} \\ \boldsymbol{S}_{\mathrm{M,y}} = -\frac{\mu}{K_{\mathrm{perm}}^{\mathrm{T}}} U_{\mathrm{y}} - K_{\mathrm{loss}}^{\mathrm{T}} \frac{\rho}{2} |\boldsymbol{U}| U_{\mathrm{y}} \\ \boldsymbol{S}_{\mathrm{M,z}} = -\frac{\mu}{K_{\mathrm{perm}}^{\mathrm{T}}} U_{\mathrm{z}} - K_{\mathrm{loss}}^{\mathrm{T}} \frac{\rho}{2} |\boldsymbol{U}| U_{\mathrm{z}} \end{cases}$$

Discharge Computation

- Non-viscous flow
- Use only the duct geometry
- 16 million elements (3, 5 or 7 Hkt model)

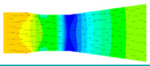

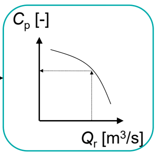

Turbine Discharge Computations

- Using the hydrokinetic turbine model

The simulation using the model overpredict the discharge by 5-10%.

Hkt ID	1	2	3	4	5	6	7
Discharge [Q/Q_{ref}]	1.25	1.26	1.29	1.29	1.29	1.02	1.03
Discharge [$Q/(Q_1+Q_2)$]	1.00	1.00	1.02	1.02	1.02	0.77	0.78

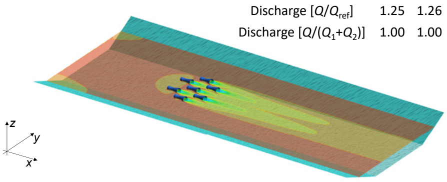

- Using the real geometry of the hydrokinetic turbine

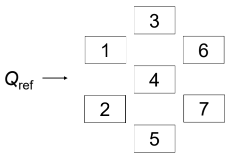

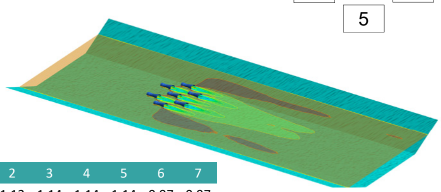

Hkt ID	1	2	3	4	5	6	7
Discharge [Q/Q_{ref}]	1.12	1.12	1.14	1.14	1.14	0.97	0.97
Discharge [$Q/(Q_1+Q_2)$]	1.00	1.00	1.01	1.01	1.01	0.87	0.87

Similar discharge trend between both simulation.

Farm Configurations

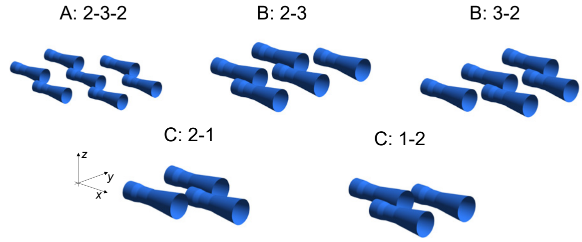

Configuration	Power Max [kW]	Diameter [m]	Length [m]
A	1.4	1.0	4.1
B	2.0	1.4	5.8
C	3.3	1.6	6.5

Results

Configuration	2-3-2	3-2	2-3	2-1	1-2
Estimated Power Max [kW]	9.51	10.24	10.21	10.07	10.04

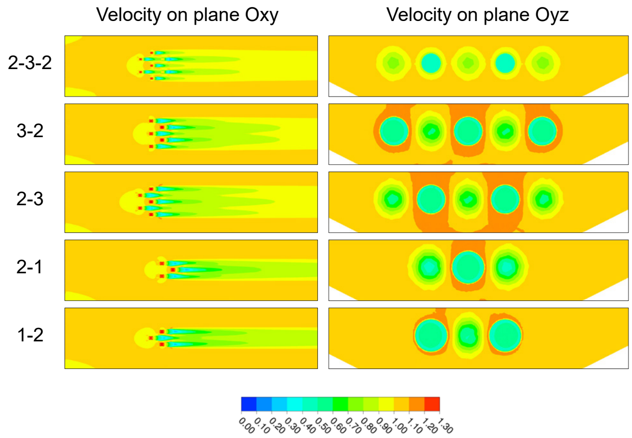

Conclusions

- The use of CFD analysis with a hydrokinetic turbine model allowed us to estimate cost-effectively the performance of a farm.
- 5 different configurations were analysed. The suitable ones are a configuration with 5 hydrokinetic turbines.
- For a final assessment, a full unsteady simulation will be required.

Schweizerische Eidgenossenschaft
Confédération suisse
Confederazione Svizzera
Confederaziun svizra
Office fédéral de l'énergie OFEN
the ark
STAHLEINBAU
SIL SERVICES INDUSTRIELS LAUSANNE
SWISS

References

[1] C. Münch, A. Gaspoz, S. Richard, V. Hasmatuchi, N. Brunner, 2017, "New prototype of a kinetic turbine for artificial channels". Simhydro Conference, Nice, 14-16 June.

[2] V. Hasmatuchi, A. Gaspoz, L. Rapillard, N. Brunner, S. Richard, S. Chevailler, C. Münch-Alligné, 2016, "Open-air laboratory for a new isokinetic turbine prototype". Annual conference, SCCER SoE, Sion.

[3] W. M. J. Batten, M. E. Harrison, A. S. Bahaj, 2013, "Accuracy of the actuator disc-RANS approach for predicting the performance and wake of tidal turbines". Phil Trans R Soc A 371: 20120293.

SCCER SoE
SWISS COMPETENCE CENTER for ENERGY RESEARCH
SUPPLY of ELECTRICITY

SCCER-SoE Annual Conference 2018

UNIVERSITÉ DE NEUCHÂTEL

GEO ENERGIE SUISSE

Supported by:
Schweizerische Eidgenossenschaft
Confédération suisse
Confederazione Svizzera
Confederaziun svizra
Swiss Confederation
Innosuisse – Swiss Innovation Agency

Calibration of borehole failure models using inverse problem methods

Asmae Dahrabou(1), Benoît Valley(1), Andres Alcolea(2), Florentin Ladner(2), Frédéric Guinot(2), Peter Meier(2)
(1) Centre for Hydrogeology and Geothermics, University of Neuchâtel,Emile-Argand 11, 2000-Neuchâtel, Switzerland.
(2) Geo-Energie Suisse AG, Reitergasse 11, 8004 Zürich, Switzerland.

I- Project context and objectives

In the frame of a CTI-project, the CHYN and Geo-Energie Suisse AG are developing a workflow and associated software tools that allow a fast decision-making process for selecting an optimal well trajectory while drilling deep inclined wells for EGS-projects. The goal is to minimize borehole instabilities as it enhances drilling performance and maximize the intersection with natural fractures because it increases overall productivity or injectivity of the well. The specificity of the workflow is that it applies to crystalline rocks and includes an uncertainty and risk assessment framework.

II- Calibration study by using inverse problem method

The main challenge in these analyses is that the strength and stress profiles are unknown independently. Calibration of a geomechanical model on the observed borehole failure has been performed using data from the Basel Geothermal well BS-1 and inverse problem method (PEST: Parameter ESTimation software).

2.1- Model sensitivity to individual measurements

A sensitivity study performed on data from the well BS-1 (DHM project Basel) by using PEST showed that the most influential parameters on borehole stability are the magnitude of the maximum and minimum horizontal stresses, S_{Hmax}, S_{hmin}, the uniaxial compressive strength, UCS, and the internal borehole pressure P_{mud}

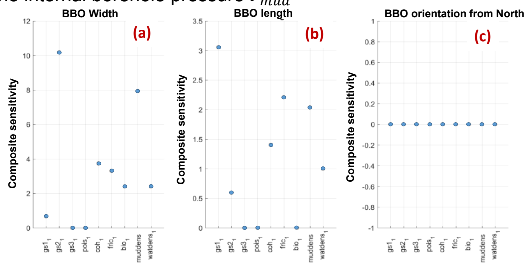

Figure 1. Calculated sensitivity of (a) borehole breakout width, (b) breakout length and (c) breakout orientation with respect to the geographical North by using PEST. The studied inputs are the gradient of the maximum, intermediate and minimum principal effective stresses respectively g_{s1}, g_{s2}, g_{s3}, Poisson ratio, the cohesion, the internal frictional angle, the Biot coefficient, mud and water densities.

2.2- The geomechanical model to calibrate

In a first approximation, a purely elasto-brittle analytical solution in combination with Mohr-Coulomb failure criterion were used. Three borehole failure indicators were used so far: the breakout width, the breakout penetration and the cross-sectional area.

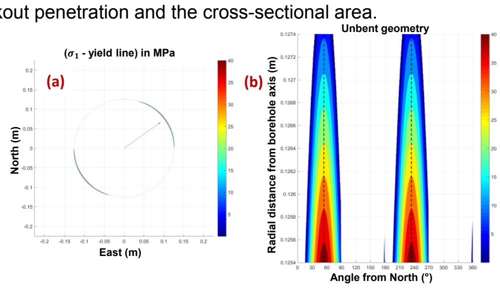

Figure 2. (a) Calculated failure in BS-1 hole at z=3500m. The blue arrow corresponds to the borehole breakout orientation (54° from the geographical North) that aligns with the orientation of S_{hmin}, the minimum horizontal principal stress. (b) Unbent spalled zone, computed in (a). The plotted geometry corresponds to the failed zone based on Mohr-Coulomb failure criterion (σ_1 - yield line) in MPa.

2.3- First results from PEST

Marquardt algorithm aims at minimizing an objective function F that relates measurements, model parameters, prior information and their weights.

F=

$$\underbrace{\sum_{i=n_w}(\gamma_w(w_i-w_i^*)^2}_{\text{Contribution of breakout width measurements}}+\underbrace{\sum_{i=n_l}(\gamma_l(l_i-l_i^*)^2}_{\text{Contribution of breakout length measurements}}+\underbrace{\sum_{i=n_\theta}(\gamma_\theta(\theta_i-\theta_i^*)^2}_{\text{Contribution of breakout width orientation}}+\underbrace{\sum_{i=n_p}(\gamma_p(p_i-p_i^*)^2}_{\text{Contribution of prior information}}$$

2.3.1- Objective function computation

The total objective function F as well as the contribution made to this latter by measurements and prior information were computed for several iterations. If the plotted objective function is fluctuating, this means that we have an instability problem of our model parameters.

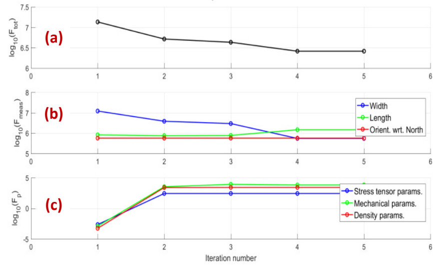

Figure 3. (a) Computed total objective function F and (b) the contribution of measurements (breakout width, breakout penetration and their orientation with respect to the geographocal North) and (b) prior information (stress tensor, mechanical and density parameters) to F.

2.3.2- Residuals of measurements after calibration

In order to check if our model leads to a good match with observations, residuals were calculated.

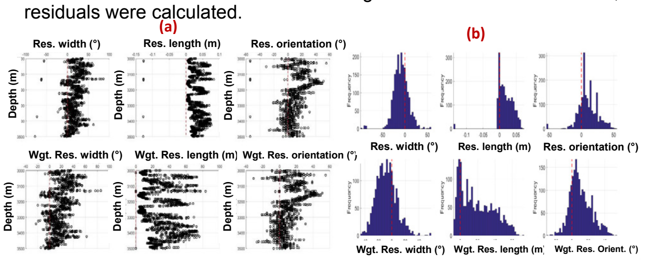

Figure 4. (a) Residuals of borehole breakout width [°], penetration [mm] and orientation with respect to the North [°] are plotted Vs. the depth [m]. (b) Histograms corresponding to each residual computed in (a).

2.3.3- Posterior covariance and correlation of parameters

If two parameters we want to estimate are highly correlated, this dependence causes the confidence intervals of the parameters to be larger than they would have been if they were independent.

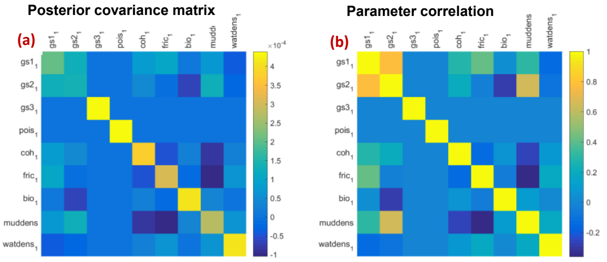

Figure 5. (a) Computed posterior covariance of parameters after calibration, (b) Computed correlation between model parameters.

III- Conclusions

- UCS and S_{Hmax} (maximum horizontal principal stresses) are the parameters the most influential on failure computation.
- High computed residuals means that we are either overestimating or underestimating our model parameters.
- If two parameters we want to estimate are highly correlated, this dependence causes the confidence intervals of the parameters to be larger than they would have been if they were independent.
- The diagonal elements of the covariance matrix are eventually high, which means that the confidence interval of the estimated parameters are very large. This means that our model is not well calibrated yet.

SCCER SoE
SWISS COMPETENCE CENTER for ENERGY RESEARCH
SUPPLY of ELECTRICITY

SCCER-SoE Annual Conference 2018

Supported by:
Schweizerische Eidgenossenschaft
Confédération suisse
Confederazione Svizzera
Confederaziun svizra
Swiss Confederation
Innosuisse – Swiss Innovation Agency

Boreholes Stability Issues in Ultra-Deep Geothermal Production

Antonio Salazar V., Leonid Germanovich, Carlo Rabaiotti, Paul Hardegger & Hansruedi Schneider

Introduction

Ultra-deep geothermal energy production is a promising source of clean energy. It is available everywhere and has the potential to supply the world's energetic needs.

The natural geothermal gradient is approximately 30°C per km. Economically feasible geothermal energy production needs rock temperatures in the range of 200° - 300° C. Therefore drilling of deep to ultra-deep boreholes (6 - 10km) is a prerequisite to successfully harvest geothermal energy in the geologic setting of Switzerland.

The objective is to physically and numerically analyze the wellbore short- and long-term stability, improving existing constitutive models to be able to realistically simulate the rock mass behavior under high pressure and high temperature conditions.

PT Triaxial device

The University of Applied Sciences in Rapperswil (HSR) has developed (with Wille AG) a unique testing device, which allows to apply a confining pressure of up to 200 MPa (2'000 bar) and a maximum axial load of 20'000 KN (Fig. 2). The tests can be performed either stress or strain controlled. An outside heating jacket allows to increase the sample's temperature up to 250° C. The apparatus can accommodate samples up to 7 cm in diameter with a corresponding length of 14 cm (Fig. 1a and 1b).
These unique features allow to impose in situ stress and temperature conditions on rock specimen corresponding to depths down to 8 km.

Figure 1a: Granite intact samples from Wassen.

Figure 1b: Tested sample under 200 MPa and 200°C.

Figure 2: High PT triaxial device with heating jacket.

Distributed Fibre Optic measurement

The radial and vertical strains of the rock samples, as well as temperature, are obtained by means of distributed fibre optic measurements. The readings are carry out adopting SWI technology with the commercial device OBR 4600 [1]. The cable is glued to the sample's surface in different geometric shapes (lines, circles and spirals), as shown in Fig. 3. The deformation can be measured over the entire length at 5 mm intervals (resolution) with a precision of 1 micro strain.

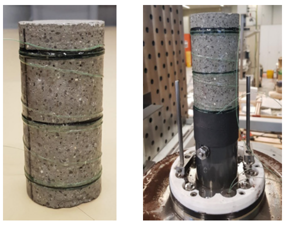

Figure 3: Fiber optic instrumented samples.

Assessment of material strength

Drucker-Prager (D-P) and Mogi-Coulomb (M-C) failure criteria are presented in the following equations and depicted in Fig. 4. The M-C surface was calibrated for the Westerly Granite ([2]) and the two D-P criteria were fitted for comparison.
As can be seen, the difference is that M-C doesn't depend in the intermediate stress.

$$\tau_{oct} \le \sigma_{oct}$$

$$\tau_{oct}^{MC} = \tau_{oct}^{DP} = \sqrt{\frac{(\sigma_1-\sigma_2)^2+(\sigma_2-\sigma_3)^2+(\sigma_1-\sigma_3)^2}{6}}$$

$$\sigma_{oct}^{MC} = A + B(\sigma_1 + \sigma_3)$$

$$\sigma_{oct}^{DP} = A' + B'(\sigma_1 + \sigma_2 + \sigma_3)$$

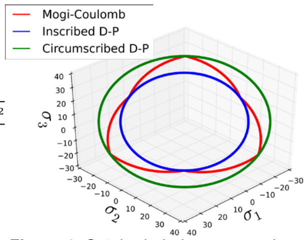

Figure 4: Octahedral-plane comparison.

Fig. 5 shows the difference between τ_{oct} and σ_{oct} ("safety factor"), when considering the criteria depicted in Fig. 4 and the stress from the analytical solution of a borehole in a homogeneous semi-infinite space. As can be seen, the circumscribed D-P can't predict the failure (Fig 5a), instead the safety factor increases with depth. On the other hand M-C apparently predicts a more realistic failure (Fig. 5c) than the inscribed D-P (Fig. 5b).

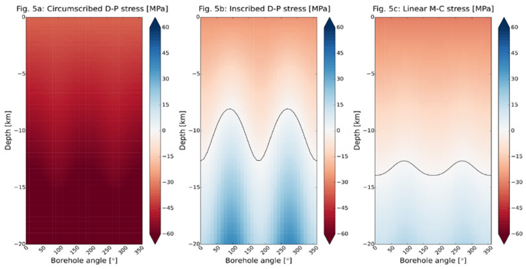

Figure 5a, 5b and 5c: $\sigma_{oct} - \tau_{oct}$ ("safety factor") for D-P and M-C criteria. Black line represent failure.

Radius of influence

Figure 6 and the following equation represent the analytical solution for the temperature of an infinite plane while extracting constant heat at a point, based on real granite properties [3]. As can be seen the temperature gradient will cause additional stresses in the rock mass, therefore it is important to evaluate the borehole stability not only due stress redistribution as a result of the drilling operation but also because of heat flow.

$$T = \frac{q}{4\pi k}\int_{r^2/4Dt}^{\infty} \frac{e^{-u}}{u}\,du$$

$t = time$
$r = distance\ from\ the\ point$
$k = thermal\ conductivity$
$D = thermal\ diffusivity$

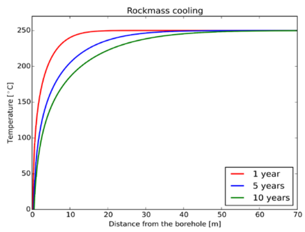

Figure 6: Rock mass temperature evolution.

References

[1] Hauswirth, D. (2015). A Study of the Novel Approaches to Soil Displacement Monitoring Using Distributed Fiber Optic Strain Sensing (Doctoral dissertation, ETH Zurich).
[2] Al-Ajmi, A. M., & Zimmerman, R. W. (2005). Relation between the Mogi and the Coulomb failure criteria. *International Journal of Rock Mechanics and Mining Sciences*, *42*(3), 431-439.
[3] Kant, M. A. et all (2017). Thermal properties of Central Aare granite for temperatures up to 500° C: Irreversible changes due to thermal crack formation. *Geophysical Research Letters*, *44*(2), 771-776.

SCCER-SoE Annual Conference 2018

SWISS COMPETENCE CENTER for ENERGY RESEARCH
SUPPLY of ELECTRICITY

LMH Laboratory for Hydraulic Machines

ÉCOLE POLYTECHNIQUE FÉDÉRALE DE LAUSANNE

Supported by:
Schweizerische Eidgenossenschaft
Confédération suisse
Confederazione Svizzera
Confederaziun svizra

Swiss Confederation

Innosuisse – Swiss Innovation Agency

Empirical model for the estimation of a Francis turbine complete characteristic curves

J. Gomes, L. Andolfatto, F. Avellan

Motivation

- The **Energy Strategy 2050**: more energy generation from renewable sources;
- In Switzerland, **many hydropower plants can be upgraded or rehabilitated** therefore generating more power with the same amount of water **[1]**;
- Feasibility studies, such as those for upgrading or rehabilitating the power plants, require estimated performance data for turbines that do not exist yet.
- Being able to properly estimate the turbine characteristics and optimize the project from the very beginning is the added-value of this research work

RENOV Hydro

The RenovHydro CTI project no. 19343.1 PFIW-IW will create a **decision making assistant for hydropower project potential evaluation and optimization**.

- 3 years project, started in Dec. 2016;
- Empirical models for the turbine characteristics estimation inside the Work Package 1 (Francis, Pelton and Kaplan turbine types);
- Partners:

groupe e, Power Vision Engineering, FMV, EPFL ÉCOLE POLYTECHNIQUE FÉDÉRALE DE LAUSANNE

Typical Francis Turbine Characteristics

Discharge Characteristics

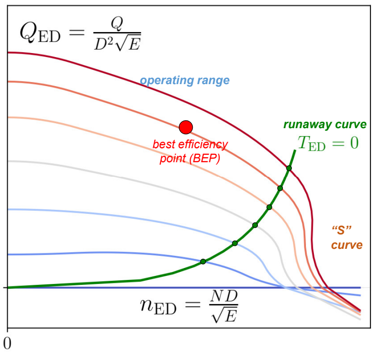

Torque Characteristics

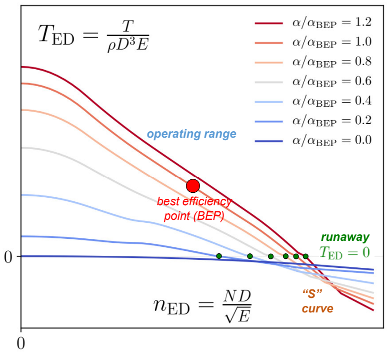

Methodology

- Data available at the *Laboratory for Hydraulic Machines* is used to defined the parameters of the empirical model.
- The turbine specific speed ν and the position of the best efficiency point are used to estimate the complete characteristics.

$$\nu = n_{ED_{BEP}} \sqrt{Q_{ED_{BEP}}}$$

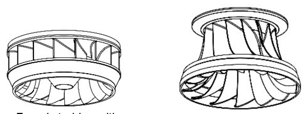

Francis turbine with low specific speed

Francis turbine with high specific speed

operating range · *runaway curve* · *"S" curve*

- Empirical model to estimate the ***normalized guide vanes angle***. Available data is used to define the 10 required parameters through squared error minimization.

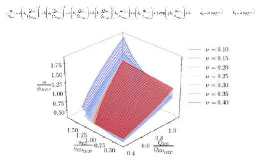

- The ***peak efficiency*** value is estimated according to the turbine year of commissioning, specific speed and runner diameter (see ref. [2]).

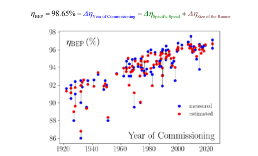

- The empirical model to predict the ***runaway curve*** where torque is zero contains 6 parameters, also defined through error minimization.

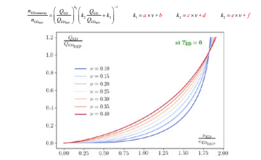

- After the runaway curve, 3 possible types of ***"S" curves*** are assumed: *stable, critical* and *unstable*.

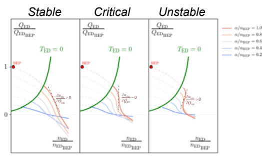

- Another empirical model estimates the loss in efficiency as the turbine operates away from the *best efficiency point* (BEP). This empirical model that calculates the ***normalized efficiency*** is based on the combination of Hermite polynomials and a standardization function.

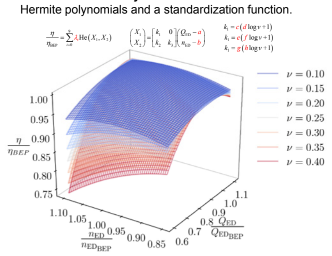

Discharge Characteristics are defined

$$T_{ED} = \frac{1}{2\pi n_{ED}} \times Q_{ED} \times \eta_{BEP} \times \frac{\eta}{\eta_{BEP}}$$

Torque Characteristics are defined

Conclusion

By means of a combination of empirical models trained with measurements from a large number of different Francis turbines, a procedure for the estimation of any Francis turbine discharge and torque characteristics has been developed.

This empirical model created inside the RenovHydro Project will be used in an optimization loop that searches for the best combination of electro-mechanical equipment, civil engineering components and ancillary services to be applied to future generating units.

References

[1] – Association Suisse pour l'Aménagement des eaux, 2012 -*Droit de retour et renouvellement de concession des centrales hydroélectriques*
[2] – Gordon, J. L., 2001. - *Hydraulic Turbine Efficiency*. Canadian Journal of Civil Engineering, 28(2), pp. 238-253

SCCER SoE
SWISS COMPETENCE CENTER for ENERGY RESEARCH
SUPPLY of ELECTRICITY

SCCER-SoE Annual Conference 2018

LMH Laboratory for Hydraulic Machines

ÉCOLE POLYTECHNIQUE FÉDÉRALE DE LAUSANNE

Supported by:
Schweizerische Eidgenossenschaft
Confédération suisse
Confederazione Svizzera
Confederaziun svizra
Swiss Confederation
Innosuisse – Swiss Innovation Agency

Cavitation modelling in GPU-SPHEROS

Audrey Maertens, Ebrahim Jahanbakhsh, François Avellan

Cavitation in hydraulic machines

- High velocities encountered in hydraulic machines can lead to cavitation.
- Cavitation causes decreased efficiency, vibrations and erosion.
- Cavitation often takes the form of clouds or ropes.
- The collapse of cavitation bubbles locally causes very high pressures that can damage the turbine.

Cavitation vortex ropes in the draft tube of a Francis turbine at part load operation

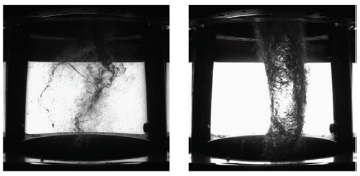

(a) $Q_{ED}/Q^*_{ED} = 0.80$ (b) $Q_{ED}/Q^*_{ED} = 0.64$

A. Favrel et al., *Journal of Hydraulic Research*, 2018.

Crater produced by the collapse of a single cavitation bubble in a Francis turbine

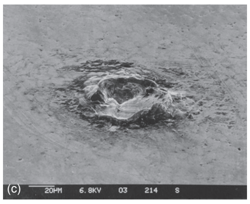

A. Karimi and F. Avellan, *Wear*, 1986.

Barotropic equation of state

- The influence of thermal effects are omitted.
- A barotropic equation of state (EOS) is constructed as a piecewise function.
- The Murnaghan-Tait equation of state is used for the liquid phase.
- The isentropic gas equation of state is used for the vapor phase.
- The Wallis sound speed for a two-phase mixture is used to define the EOS in the mixture.

$$p(\rho) = \begin{cases} B_v \left(\dfrac{\rho}{\rho_v}\right)^{\gamma_v} & \text{if } \rho \le \rho_v, \\ p_l - B_v \gamma_v \ln\left[1 + \dfrac{B_l \gamma_l}{B_v \gamma_v}\left(\dfrac{\rho_l}{\rho} - 1\right)\right] & \text{if } \rho_v < \rho < \rho_l, \\ p_l + B_l \left[\left(\dfrac{\rho}{\rho_l}\right)^{\gamma_l} - 1\right] & \text{if } \rho_l < \rho. \end{cases}$$

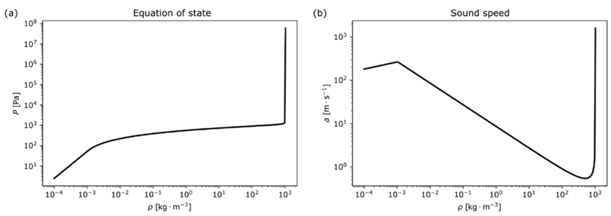

Riemann formulation for flows with discontinuities

- Cavitating flows are characterized by discontinuities, large density ratios, and shock waves.
- The conservation laws are recast into a Riemann problem:
$$\frac{\partial \boldsymbol{U}}{\partial t} + \nabla \cdot \boldsymbol{F}(\boldsymbol{U}) = \nabla \cdot \boldsymbol{D}(\boldsymbol{U}, \nabla \boldsymbol{U})$$
- Kurganov's central-upwind scheme is revisited and adapted to FVPM: $\frac{\mathrm{d}}{\mathrm{d}t}\left(\overline{\boldsymbol{U}}_i(t) V_i(t)\right) = -\sum_{j \neq i} \boldsymbol{H}_{ij}(t)$
- Fluxes are computed as: $\boldsymbol{H}_{ij} = \boldsymbol{G}_{ij} \cdot \boldsymbol{\Gamma}_{ij} - \boldsymbol{G}_{ji} \cdot \boldsymbol{\Gamma}_{ji}$
- Where $\boldsymbol{G}_{ij} = \widetilde{\boldsymbol{F}}_{ij} - \dot{\boldsymbol{x}}_j \widetilde{U}_{ij} - \boldsymbol{R}_{ij} - \boldsymbol{D}_{ij}$ includes:
  - Conservative flux $\widetilde{\boldsymbol{F}}_{ij} = \dfrac{a^+_{ij} - \dot{\boldsymbol{x}}_j \cdot \boldsymbol{n}_{ij}}{a^+_{ij} - a^-_{ij}} \boldsymbol{F}(\boldsymbol{U}^-_{ij}) - \dfrac{a^-_{ij} - \dot{\boldsymbol{x}}_j \cdot \boldsymbol{n}_{ij}}{a^+_{ij} - a^-_{ij}} \boldsymbol{F}(\boldsymbol{U}^+_{ij})$
  - Conserved variables $\widetilde{U}_{ij} = \dfrac{a^+_{ij}}{a^+_{ij} - a^-_{ij}} \boldsymbol{U}^+_{ij} - \dfrac{a^-_{ij}}{a^+_{ij} - a^-_{ij}} \boldsymbol{U}^-_{ij}$
  - Smoothing flux $\boldsymbol{R}_{ij} = \dfrac{a^+_{ij} a^-_{ij}}{a^+_{ij} - a^-_{ij}} \left(\boldsymbol{U}^+_{ij} - \boldsymbol{U}^-_{ij}\right) \otimes \boldsymbol{n}_{ij}$
  - Dissipative flux $\boldsymbol{D}_{ij}$

Cavitation cloud through a Venturi tube

- Simulation of a Venturi tube with pressure boundary conditions.
- $P_{in} = 0.6$ MPa and $P_{out} = 0.12$ MPa.
- Tube length is 40 mm, diameter gradually decreases from 3.6 mm to 1.19 mm and increases again.
- The constriction causes a flow acceleration and pressure drop, creating a cavitation cloud.
- The cloud detaches and bubble collapses cause pressure spikes.

Bubble collapse near a wall

- Low pressure vapor bubble inside a high pressure fluid attached to a wall.
- Density ratio greater than 1000 is easily handled and sharpness is maintained.
- After initial shrinking of the bubble, a re-entrant micro-jet forms toward the wall and the bubble becomes a ring.
- The collapse of the ring generates a very large pressure with pressure waves that meet in the center.